JPR Advance Access published May 22, 2014

Journal of
Plankton Research

plankt.oxfordjournals.org

J. Plankton Res. (2014) 0(0): 1–18. doi:10.1093/plankt/fbu042

Metabolic state along a summer north–south transect near the Antarctic Peninsula: a size spectra approach

CRISTINA GARCÍA-MUÑOZ[1]*, CARLOS M. GARCÍA[2], LUIS M. LUBIÁN[1], ÁNGEL LÓPEZ-URRUTIA[3], SANTIAGO HERNÁNDEZ-LEÓN[4] AND JULIA AMENEIRO[5]

[1]DEPARTAMENTO DE ECOLOGÍA Y GESTIÓN COSTERA, INSTITUTO DE CIENCIAS MARINAS DE ANDALUCÍA (ICMAN-CSIC), PUERTO REAL, CÁDIZ, SPAIN, [2]DEPARTAMENTO DE BIOLOGÍA, FACULTAD DE CIENCIAS DEL MAR Y AMBIENTALES, UNIVERSIDAD DE CÁDIZ, PUERTO REAL, CÁDIZ, SPAIN, [3]CENTRO OCEANOGRÁFICO DE GIJÓN, INSTITUTO ESPAÑOL DE OCEANOGRAFÍA, GIJÓN, ASTURIAS, SPAIN, [4]INSTITUTO DE OCEANOGRAFÍA Y CAMBIO GLOBAL, UNIVERSIDAD DE LAS PALMAS DE GRAN CANARIA, LAS PALMAS DE GRAN CANARIA, ISLAS CANARIAS, SPAIN AND [5]DEPARTAMENTO DE ECOLOXÍA E BIOLOXÍA ANIMAL, FACULTADE DE CIENCIAS DO MAR, UNIVERSIDADE DE VIGO, VIGO, SPAIN

*CORRESPONDING AUTHOR. cristina.garcia@icman.csic.es

Received November 13, 2013; accepted April 19, 2014

Corresponding editor: Zoe Finkel

To establish a metabolic state along a north–south transect in Antarctic waters, we approached community respiration (CR) from a combined perspective based on the metabolic theory of ecology (MTE) and the size-scaling of the whole planktonic community. A detailed analysis of a summer integrated multi-trophic normalized biomass size spectra (NBSS), from heterotrophic bacteria to zooplankton, was carried out. To acquire individual size data, different techniques were combined: flow cytometry for smaller fractions (<20 μm of equivalent spherical diameter), FlowCAM for larger nano- and microplankton and scanning and image analysis for the zooplankton fractions. The distribution of the NBSS was linear at all stations (R^2 values: 0.87–0.93) but dome-shape features appeared related to phytoplankton cell distribution which are responsible for a large fraction of microbial respiration. Generally, the region showed an autotrophic budget south of the archipelago due to gross primary production (GPP) values up to 2804 mg C m^{-2} day^{-1}, where salps could significantly contribute to the carbon export flux. Contrastingly, higher CR rates (>1000 mg C m^{-2} day^{-1}) were found at the northern stations due to a higher phytoplankton respiration activity associated with increasing sea water temperatures and a higher presence of heterotrophic organisms (microheterotrophs, chaetognaths and copepods) resulting in a net heterotrophic metabolic state (GPP/CR < 1).

KEYWORDS: metabolic state; normalized biomass size spectra; south Shetland Islands

available online at www.plankt.oxfordjournals.org

© The Author 2014. Published by Oxford University Press. All rights reserved. For permissions, please email: journals.permissions@oup.com

Downloaded from http://plankt.oxfordjournals.org/ at Southern Methodist University on August 22, 2014

INTRODUCTION

The significant contribution of the marine biota to the global carbon cycle ultimately results from the balance between gross primary production (GPP) and community respiration (CR) (Serret *et al.*, 2001a). Autotrophic communities (GPP > CR, with positive net community production (NCP)) act as sinks of CO_2 and inorganic nutrients and sources of organic matter and O_2, while heterotrophic communities (GPP < CR, NCP < 0) act as sources of CO_2 and inorganic nutrients and sinks of organic matter and O_2 (Duarte and Regaudie-de-Gioux, 2009). Thus, the estimation of NCP and the study of its dynamics and space variation constitute an important step in understanding carbon budgets. Agustí *et al.* (Agustí *et al.*, 2004) report on the basis of a comparative analysis of planktonic metabolism in the Southern Ocean (SO) that CR exceeds GPP in communities where GPP < 2.05 mmol O_2 m^{-3} day^{-1}. The existence of such thresholds is important to help delineate the area of the SO supporting net heterotrophic communities (GPP < CR).

In this context, considering the distribution of CR, we should differentiate between the metabolism of autotrophic and heterotrophic communities. Quantification of community balance is problematic due to the difficulties in measuring planktonic metabolism especially the respiration apportioned within the different trophic levels. Alternative ways to track planktonic respiration have been described in Robinson and Williams (Robinson and Williams, 2005), namely the calculation of respiration from algorithms of biomass distribution and measurements of the size distribution of respiration throughout the biomass size spectra (BSS). The combination of size spectra and allometry has been suggested as a reasonable estimation of CR across contrasting ecosystems (Quiñones *et al.*, 1994; Blanco *et al.*, 1998). In this study we tackle the CR question from a combined perspective based on the metabolic theory of ecology (MTE) and the size-scaling of the whole planktonic community. The flux rates within an ecosystem are the result of the sum of the individual rates of all its constituent organisms, which, in turn, are governed by the combined effects of body size and temperature not only for phytoplankton (López-Urrutia *et al.*, 2006) but also for zooplankton (Hernández-León and Ikeda, 2005). In this sense the parameters of the BSS and especially the analyses of the slopes are used to assess the state of marine ecosystems at regional and global scales (Shin *et al.*, 2005). This is a reasonable way of measuring the relationship between growth, mortality and respiration of a community (Platt and Denman, 1978). Low-productivity pelagic ecosystems close to steady state usually show linear size spectra (Rodríguez and Mullin, 1986; Quiñones *et al.*, 2003) while more productive ecosystems, that are also subject to stronger hydrodynamic forcing, can show irregularities in the size spectrum (e.g. Sprules and Munawar, 1986; García *et al.*, 1995; Reul *et al.*, 2006) both due to top-down or bottom-up processes. Furthermore, the slope of the spectrum gives an indication of the efficiency of biomass transfer to larger organisms (Gaedke, 1993) and reflects changes in the upper ocean carbon flux (San Martín, 2005).

Despite the great information that the BSS contains, only few studies have focused on the Antarctic spectrum (e.g. nekton spectrum in Rodhouse *et al.*, 1994; phytoplankton spectrum in Rodríguez *et al.*, 2002; mesozooplanton spectrum in Zhou *et al.*, 2004). Witek and Krajewska-Soltys (Witek and Krajewska-Soltys, 1989) and Tarling *et al.* (Tarling *et al.*, 2012) are the only works, to our knowledge, that emphasized a multi-trophic plankton spectrum.

To delve deeper into the study of the Antarctic BSS, a comprehensive analysis of the whole planktonic community BSS from heterotrophic bacteria (HB) to zooplankton has been developed in this manuscript, following a north–south transect crossing the South Shetland Islands (SSI) from the Drake Passage to the Antarctic Peninsula. Furthermore, a special emphasis is placed on the metabolic balance to overview local differences on both sides of the archipelago based on the respiration rates of each trophic compartment. This was with the aim of determining if the study area supports a net autotrophic or a net heterotrophic metabolic state.

METHOD

Sampling

Sampling was conducted during the *COUPLING* cruise, January 2010, on board *RV Hespérides*. The present article is based on the observations from a transect (T.1), which crossed the northern and southern regions around the SSI from the Drake Passage to the southern Bransfield Strait (Fig. 1). Vertical profiles of temperature and conductivity were performed using a Seabird 911plus conductivity–temperature–depth sensor with an additional oxygen sensor calibrated on board using an automated Winkler titration system (Metrohm 716 DMS) following WOCE protocols (Culberson, 1994). Oxygen saturation was calculated using the equations of Weiss (Weiss, 1970) as in Carrillo *et al.* (Carrillo *et al.*, 2004).

Mixed layer depth (MLD) was inferred from temperature and salinity profiles using the algorithm of Kara *et al.* (Kara *et al.*, 2000). For each station, a vertical light attenuation coefficient K_d (m^{-1}) was calculated by measuring

Downloaded from http://plankt.oxfordjournals.org/ at Southern Methodist University on August 22, 2014

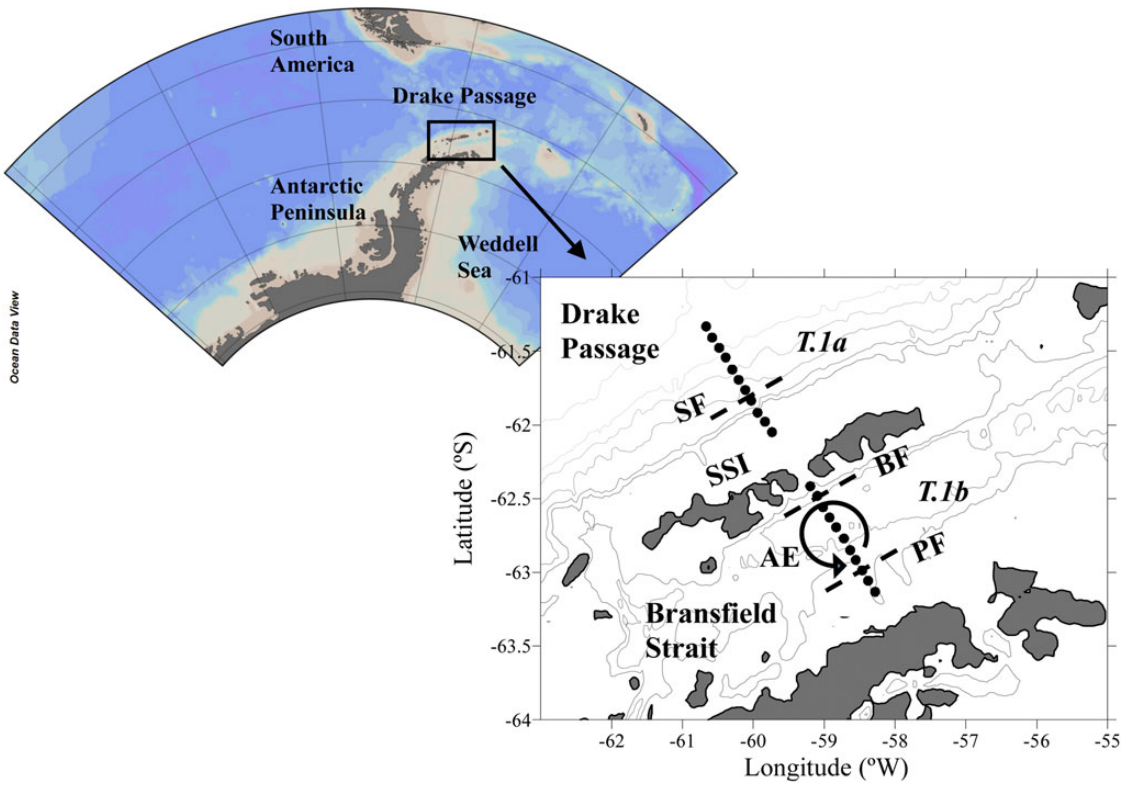

Fig. 1. Location of sampling stations across the South Shetland Islands (SSI). AE: anti-cyclonic eddy, BF: Bransfield Front, PF: Peninsula Front, SF: Shetland Front. Further details of the mesoscale structures in García-Muñoz *et al.* (García-Muñoz *et al.*, 2013a).

the photosynthetically active radiation (PAR, 400–700 nm) values at 1 m depth intervals in the water column with a hemispherical quantum sensor (CI PAR, Chelsea Instruments, relative spectral sensitivity flat to ± 3% from 450 to 700 nm).

The euphotic zone depth (Zeu) was defined as the depth at which the light intensity was attenuated to 1% of the value just below the surface, and was calculated as $\ln(0.01)/K_d$.

At each station, water sampling was performed at six fixed depths (5, 10, 25, 50, 75 and 100 m) including the depth of the fluorescence maximum, using a rosette system of 24 12-L Niskin bottles. Whole water samples for flow cytometry were fixed with paraformaldehyde and glutaraldehyde (1 + 0.05% final concentrations). Nano- and microplankton samples (5 L) were filtered through a 10-μm mesh to a final volume of 100 mL, fixed with buffered formaldehyde (4% final concentration) and stored in amber glass flasks. Meso- and macrozooplankton were sampled with a MOCNESS net equipped with seven nets (including five double nets). Mesh size for the outer net was 250 μm. At most stations, MOCNESS was towed in oblique hauls from 10–40, 40–70, 70–100, 100–200, 200–300 and 300–400 m. Transmission by underwater sensors on the MOCNESS through conducting cable to the deck yielded output of depth, frame angle, volume filtered and net closing response at 1-s intervals. Towing speed was ∼2 knots and the mean tow duration was 40 min 14 s ± 6 min 58 s (SE). The material retained was fixed (4% formaldehyde) and stored in plastic bottles.

Plankton analysis

Three complementary techniques (Flow cytometry, FlowCAM and scanning-based image analysis) were used in a way that allowed a large size-range overlap. Pico- and nanoplankton were counted on board using a FACSCalibur cytometer (Becton Dickinson) immediately after water sampling. SYTO-13 staining was used for the flow cytometry determination of the heterotrophic bacterioplankton and the heterotrophic nanoflagellate abundance following the method of del Giorgio *et al.* (del Giorgio *et al.*, 1996) and Christaki *et al.* (Christaki *et al.*, 2011), respectively. Although *Archaea* could be quantified as well with the first method, their abundance in surface waters (0–100 m) accounted for 1% of the total picoplankton assemblage (Church *et al.*, 2003) during the

Downloaded from http://plankt.oxfordjournals.org/ at Southern Methodist University on August 22, 2014

austral summer, thus heterotrophic prokaryotes mainly consisted of bacterioplankton. They were all included in the same octave (0.49–0.62 μm, equivalent spherical diameter, ESD) due to the low precision in estimating their size by flow cytometry and constant volume reported for Antarctic waters (Delille, 2003). Biovolume for the rest of the cells was estimated through the calibration of the side scatter signal with seven sized plankton cultures (García-Muñoz *et al.*, 2013a). We did not attempt to make any corrections due to the effect of fixation, but to minimize this effect flow cytometry samples were analysed immediately after their collection. Photosynthetic prokaryotic picoplankton was almost absent during the whole cruise. Heterotrophic nanoflagellates were triggered using different fluorescence thresholds as proposed by Zubkov *et al.* (Zubkov *et al.*, 2007) and Christaki *et al.* (Christaki *et al.*, 2011). Further details of HB and autotrophic nanoplankton discrimination are given in García-Muñoz (García-Muñoz, 2014) and García-Muñoz *et al.* (García-Muñoz *et al.*, 2013a), respectively.

Larger nanoplankton and microplankton were counted and measured using a FlowCAM® (Fluid Imaging Technologies) in auto-trigger mode. Samples were pumped first through a chamber of 3.0 mm × 0.3 mm cross section, using a ×4 objective for 50 min, to analyse the 64–200 μm size fraction. Then, samples were filtered through 100-μm mesh and pumped using a chamber of 2.0 mm × 0.1 mm and a ×10 objective for 40 min, to analyse the 16–100 μm size fraction. We assumed that particles were randomly distributed within the chambers. Acquisition times were selected in accordance with the recommendations of Álvarez *et al.* (Álvarez *et al.*, 2011) to obtain a good representation of the different size ranges. Invalid recordings (i.e. bubbles, repeated images) were removed from the image database. Differentiation between phytoplankton and non-phytoplankton particles (i.e. debris, heterotrophs) was done through visual recognition. Biovolume was calculated using the area-based diameter (ABD) of each cell with a previous volume correction for fixed samples (Menden-Deuer *et al.*, 2001).

Meso- and macrozooplankton samples were strained onto a 200-μm mesh screen and rinsed into a Folsom splitter using artificial seawater. Gelatinous plankton was previously removed from the sample and treated separately due to the high abundance found. Each sample was split to obtain fractions with homogeneous abundances and poured directly into a tray for scanning. Any overlapping organisms were manually separated before the sample was digitized. Samples were scanned with an Epson Perfection 4990 Photo colour flatbed scanner. Image analysis was performed using Zooimage software (http://www.sciviews.org/Zoo/PhytoImage) following Bachiller and Fernandes (Bachiller and Fernandes, 2011). The biovolume of each organism was assumed to be equivalent to that of the corresponding sphere using the equivalent circular diameter (ECD) output. Samples were processed more than a year after their collection therefore body length was corrected due to shrinkage as in Black and Dodson (Black and Dodson, 2003).

For cells smaller than 200 μm ESD, biovolume was converted to carbon biomass using the conversion equations given by Menden-Deuer and Lessard (Menden-Deuer and Lessard, 2000). For meso- and macrozooplankton, individual biomass was estimated by using the Alcaraz *et al.* (Alcaraz *et al.*, 2003) equations, as previously in the study area (see Calbet *et al.*, 2005).

Building size spectra

Size classes were established following a geometric $2n$ series (Sheldon *et al.*, 1972). The organisms were grouped into 47 volume classes without any special taxonomic preference since the sub-samples represented the average composition of samples. With this partition, the amplitude of the size class (Δw) coincides with its lower limit (w). The normalized biomass in each class ($\beta(w_i)$) can be calculated from biomass, here biovolume (B) as:

$$\beta(w_i) = [B(w, w + \Delta w)]/\Delta w \quad (1)$$

When data are plotted on a log–log axis, the relationship is linear and it is possible to obtain the overall parameterization of the normalized biomass size spectra (NBSS) (Platt and Denman, 1978) (Fig. 2):

$$\log \beta(w) = a + b \log w \quad (2)$$

where a (intercept) and b (slope) are the parameters of the fitted line.

We defined a size class without detectable biomass as a "biological gap" in the spectrum. To include these gaps in the NBSS, we applied the method proposed by Tittel *et al.* (Tittel *et al.*, 1998) and followed by Cózar *et al.* (Cózar *et al.*, 2003) ($0.01B$) for sizes over 20 μm ESD. For those cells in the picoplankton range (0.2–2 μm ESD), we decided to apply a more restricted method ($0.001B$) close to the detection limit of the flow cytometer used (2 cells mL^{-1}) due to the low abundance of photosynthetic prokaryotic picoplankton in the study area. We defined as a "methodological gap" in the spectrum the discontinuity between 200 and 250 μm due to non-overlapping techniques used to collect samples in this size range. Larger errors and poor estimations of abundance due to scarcer number of observations may be expected at the end of the size spectrum, leading to either under or overestimation. Therefore, we have limited the spectrum at a maximum ESD of 3.2 cm, even though larger salps were

Downloaded from http://plankt.oxfordjournals.org/ at Southern Methodist University on August 22, 2014

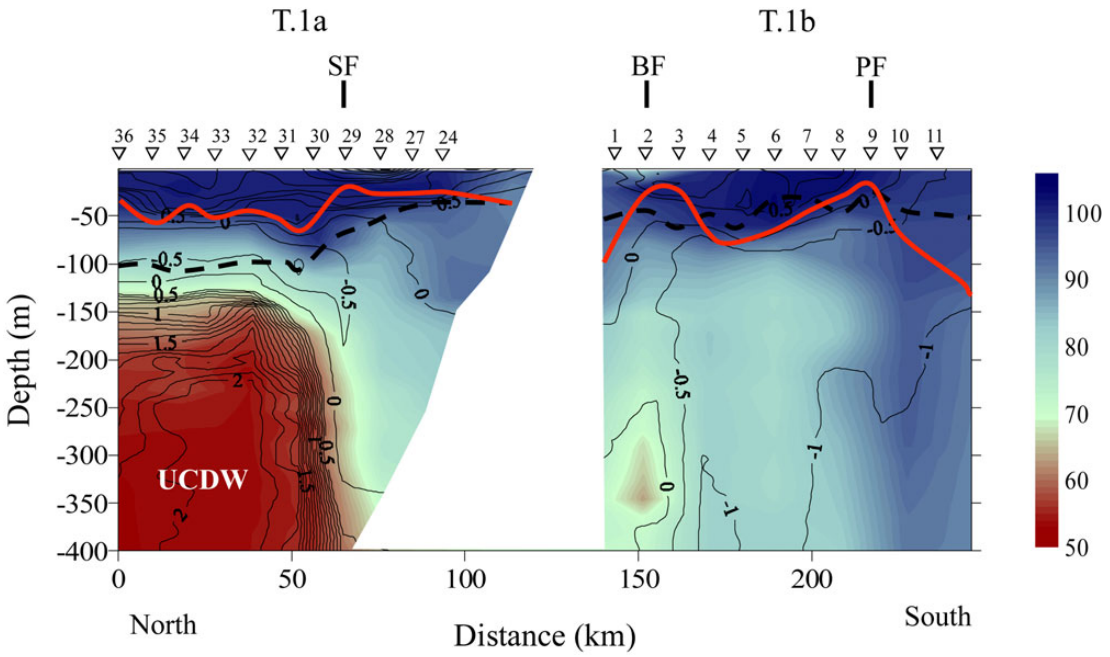

Fig. 2. Percentage of oxygen saturation ($\%O_2$) (surface down to 400 m) along the transect. Isolines represent isotherms. UCDW: upper circumpolar deep water. Thick line is the MLD. Dashed line is the Zeu. The locations of the fronts are indicated above the figure: BF: Bransfield Front, PF: Peninsula Front, SF: Shetland Front.

Table I: Summary of oceanographic and biological parameters measured along the transect

Station	Latitude (°S)	SST (°C)	MLD (m)	Zeu (m)	Intercept	Slope	R^2	GPP (mg C m^{-2} day^{-1})	CR (mg C m^{-2} day^{-1})	GPP/CR
36	−61.33	1.09	32.6	**103.6**	10.70	−0.83	0.91	1318	1406	0.94
35	−61.41	1.02	55.7	**103.9**	10.88	−0.90	0.90	1418	1499	0.95
34	−61.48	1.08	45.0	**118.3**	11.08	−0.89	0.93	1049	1346	0.78
33	−61.54	1.01	55.1	**114.3**	11.16	−0.89	0.92	909	1150	0.79
32	−61.63	0.86	51.1	**100.3**	10.81	−0.81	0.88	1383	1907	0.73
31	−61.69	0.91	55.2	**100.3**	10.90	−0.88	0.90	1051	989	1.06
30	−61.76	0.96	68.6	**110.7**	11.18	−0.91	0.91	1015	1215	0.84
29	−61.84	1.13	23.9	**75.1**	10.34	−0.80	0.87	1263	1502	0.84
28	−61.93	0.83	34.8	**60.2**	10.77	−0.90	0.90	1456	949	1.5
27	−61.98	0.86	33.0	**46.6**	10.48	−0.88	0.88	1012	805	1.26
24	−62.05	0.70	32.0	**43.3**	10.75	−0.94	0.90	1933	793	2.44
1	−62.42	0.54	**97.2**	53.5	10.64	−0.84	0.92	708	335	2.11
2	−62.48	0.66	38.2	**47.3**	10.68	−0.91	0.89	1421	401	3.55
3	−62.56	0.85	32.5	**65.8**	10.50	−0.83	0.89	2043	865	2.36
4	−62.63	0.61	**61.5**	55.0	10.62	−0.86	0.90	1006	616	1.63
5	−62.69	0.50	**78.3**	67.6	10.69	−0.85	0.89	2804	1068	2.63
6	−62.77	0.69	**61.1**	42.4	10.45	−0.79	0.87	1611	615	2.62
7	−62.85	0.55	**49.6**	45.1	10.52	−0.87	0.88	1266	575	2.20
8	−62.92	0.59	33.54	**53.0**	10.81	−0.90	0.90	2422	984	2.46
9	−62.99	0.56	18.2	**39.9**	10.29	−0.82	0.88	2028	687	2.95
10	−63.06	−0.21	**81.3**	57.0	11.17	−0.96	0.91	1617	730	2.22
11	−63.13	−0.45	**116.6**	67.8	11.83	−1.02	0.93	964	781	1.23

SST: sea surface temperature (°C), MLD: mixed layer depth (m), Zeu: euphotic depth, NBSS parameters: intercept, slope and R^2; GPP: gross primary production (mg C m^{-2} day^{-1}), CR: community respiration (mg C m^{-2} day^{-1}).
Stations sampled north of the South Shetland Islands (T.1a) have blank background whereas stations sampled south (T.1b) are shaded grey. The integration depths considered for each station are in bold.

occasionally collected. Data from bacteria to microplankton were depth integrated, by means of a trapezoidal integration, within the euphotic zone (in m) or the MLD (in m), whichever was deeper (Table I). Natural spline interpolating functions were used when the integration depth was in between two sampled standard depths (see

Downloaded from http://plankt.oxfordjournals.org/ at Southern Methodist University on August 22, 2014

Sampling section). Since zooplankton vertical migration was evident in this study area (Hernández-León *et al.*, 2001), we considered depth integration of zooplankton data from the surface down to 400 m as in Ward *et al.* (Ward *et al.*, 2012a, b).

NBSS regression analyses were carried out using least-squares (Model I) regression. For biomass size-distribution data, where the independent variable (i.e. body size) is not under the control of the investigator and is subjected to error, Model II (i.e. both variables show random variation) would be more appropriate (Laws and Archie, 1981). However, we have decided to use Model I because it permitted us to test differences between regression lines and also made the comparison with other published spectra easier as in Quiñones *et al.* (Quiñones *et al.*, 2003). Prior to the comparison of regression lines, the necessary assumption of homogeneity of variance was tested using Bartlett's test. After passing the Bartlett's test, an *F*-test for multiple comparisons among slopes and elevations and *post hoc* Tukey tests were used to evaluate if there were differences in the size structure (NBSS parameters: intercept and slope) between different stations and areas. In addition, a *t*-test was used to test if the slopes of the normalized biomass size spectra were significantly different from −1 (Sokal and Rohlf, 1981).

Metabolism: production/respiration rates

In a previous paper, García-Muñoz *et al.* (García-Muñoz *et al.*, 2013b) compared and evaluated several primary production models to obtain realistic Net primary production rates for the study region, including an allometric model based on the MTE. The authors concluded that the carbon-based primary model (CbPM) based on the chlorophyll *a*/carbon biomass ratio modulation [first described by Behrenfeld *et al.* (Behrenfeld *et al.*, 2005), and later updated by Westberry *et al.* (Westberry *et al.*, 2008)] was the best model as it made a special attempt to detect both nutrient, light and temperature modulation of NPP. Thus, the output of this model across the selected transect was used in this manuscript to further establish a metabolic state. Respiration rates were calculated on the basis of the MTE using the equations given in López-Urrutia and Morán (López-Urrutia and Morán, 2007) for HB:

$$\text{Bacterial Respiration}((\text{fg C cell}^{-1}\text{day}^{-1}))_z = 3.21 \times 10^{11} e^{-0.589/kT} \quad (3)$$

and López-Urrutia *et al.* (López-Urrutia *et al.*, 2006) for the other organisms:

$$\ln(\text{Respiration}\ (mmol\ O_2\ cell^{-1}\ day^{-1}))_z = \ln \mathcal{N}c + \alpha \times \ln(M_i) - E_a \times (1/kT) + \ln(I_z/(I_z + Km)) :$$

$$\ln(\text{Respiration}(\text{mmol O}_2\ \text{cell}^{-1}\ \text{day}^{-1}))_z = -0.76 + 0.87 \times \ln(M_i) - 0.56 \times (1/kT) \quad \text{for heterotrophs} \quad (4)$$

$$\ln(\text{Respiration}(\text{mmol O}_2\ \text{cell}^{-1}\ \text{day}^{-1}))_z = -13.18 + 1.02 \times \ln(M_i) - 0.28 \times (1/kT) + \ln(I_z/(I_z + 1.52))\ \text{for autotrophs} \quad (5)$$

where N_c is the respective normalization constant, α is the allometric exponent, M_i is the organism mass (pg C), E_a is the activation energy (eV), k is the Boltzmann's constant (8.62×10^{-5} eV K^{-1}), T is the temperature (K), K_m is the Michaelis–Menten half-saturation constant and I_z is the daily PAR at each depth (mol photons m^{-2} day^{-1}) calculated as described in García-Muñoz *et al.* (García-Muñoz *et al.*, 2013b) for the primary production MTE model. Note that the latter term was not used to calculate heterotroph respiration rates. We used a respiratory quotient of 1 for carbon conversion and summed the individual cell respiration rate at each depth to obtain mg C m^{-3} day^{-1} units. CR was calculated as the sum of the respiration rates of all the planktonic organisms considered and, finally, GPP was obtained by summing the corresponding respiration rate of the phytoplankton cells to NPP.

Non-parametric multivariate techniques were used with the PRIMER v 6.1 statistical package to discern station grouping on the basis of the NBSS slope and the metabolic balance through the GPP/CR ratio along the transect studied. A similarity matrix was constructed by means of Bray–Curtis similarity index. From this matrix, the stations were classified by the group-average sorting algorithm. Non-metric multidimensional scaling (MDS) was used to evaluate the group separation derived from the cluster analysis. Significant Pearson rank correlation vectors ($r > 0.5$, $P < 0.05$) between the log-transformed abundances and the respiration rates of the different trophic compartments and the MDS axes were overlapped.

RESULTS

Oxygen saturation and sea surface temperature

Physical features and water masses found during this cruise have been already described in detail elsewhere (Teira *et al.*, 2012; García-Muñoz *et al.*, 2013a, 2014). However, we also show sea surface temperature (SST) (Table I) in this paper due to the strong north–south

Downloaded from http://plankt.oxfordjournals.org/ at Southern Methodist University on August 22, 2014

variation detected which directly controls the metabolic rates of the whole planktonic community and even exerts a strong control on the distribution of the meso-macrozooplankton groups, as described by Loeb *et al.* (Loeb *et al.*, 2010). Warmer surface temperatures were detected at the northern stations (>1°C) while they decreased southwards reaching negative values at the end of T.1b (−0.45°C, minimum value observed). The percentage of oxygen saturation (%O_2)-linked isotherms (Fig. 2) has been chosen to interpret the biological distribution across the study area, as it is known to be a valuable tool to broadly summarize the recent history of biological activity (e.g. Serret *et al.*, 2001a). Values over 100% were detected in the upper layer (surface to 50 m) across the transect (Fig. 2). Values close to 90% were also detected at the southern end of the transect throughout the water column, where isotherms showed a sub-ductive structure and the highest MLD was detected (Table I). Low values (<70%) were found below the Zeu (Table I) in the northern stations, where the relatively warm (>0°C) and salty (>34.4) upper circumpolar deep water was located (García-Muñoz *et al.*, 2013a).

Plankton structure and abundance

Despite the ataxonomic nature of the size spectrum, it seems convenient to describe the main sized-trophic compartments that form it to further study the interactions between their abundance and metabolic rates. HB reached abundance values over 1×10^{13} cells m^{-2} along the transect (Fig. 3B). The maximum concentrations ($>2.5 \times 10^{13}$ cells m^{-2}) were recorded both in the middle of the Bransfield and in the northern SSI shelf. Phytoplankton in the nano-size range (2–20 μm ESD) (NA) predominated throughout the transect (mean ± SD: $3.3 \pm 0.8 \times 10^{11}$ cells m^{-2}) (Figs 3C and 4A), increasing southwards across T.1a. The highest abundances ($>4 \times 10^{11}$ cells m^{-2}) occurred in the middle of the Bransfield, while the lowest were detected at both edges of T.1b. Nanoheterotrophs (NH) showed a patchy distribution ranging between 0.2 and 3.5×10^{10} cells m^{-2} increasing southwards along T.1b (Fig. 3D). Their highest contribution (≈50%) to total biomass in each size class was due to larger organisms (16–20 μm ESD) (Fig. 4A).

Microplanktonic phytoplankton was mostly composed of large diatoms (50–80 μm ESD), reaching maximum concentrations at St. 33 and 30 (over 1×10^8 cells m^{-2}) in the T.1a and St. 1 and 11 in the T.1b (Fig. 3E). Nanoplanktonic and microplanktonic dinoflagellates detected with FlowCAM were considered to be autotrophic. Although FlowCAM can be used in a fluorescence mode to detect autotrophic cells, our samples were fixed and, therefore, no fluorescence measurements could be made, but pigment analyses performed with high performance liquid chromatography confirmed the presence of peridinin-containing dinoflagellates in the study area (García-Muñoz *et al.*, 2013a). Overall phytoplankton dominated the total biomass of microorganisms (over 50% of total biomass within each size range) across the spectra up to 159 μm ESD (Fig. 4A).

Microplanktonic heterotrophs (MH) showed a wide range of concentrations (9.5×10^6–9.5×10^7 cells m^{-2}) decreasing southwards (Fig. 3F). Zooplankton was always dominated by copepods, followed by chaetognaths, salps and krill. The high copepod abundance detected at the northern stations (St. 36–32, ranging between 6000 and 23 000 ind. m^{-2}), and at both edges of the T.1b (St. 1 and 11, >5800 ind. m^{-2}) (Fig. 3G) is noteworthy. The highest volumetric abundances across the whole transect were always detected in the deeper layers: 200–300 and 300–400 m, corresponding with a concentration of *Metridia gerlachei*, whereas surface layers were dominated by small copepods, mainly *Oithona sp.* (data not shown). *Salpa thompsoni* showed an opposite pattern with the highest concentrations detected in the middle of the Bransfield Strait (>300 ind. m^{-2}) (Fig. 3H). On average, copepods represented 81% of total zooplankton abundance throughout the study area. If we focus on the individuals' size distribution, copepods contributed >75% of total zooplankton abundance >2 mm, while salps contributed >80% of those organisms >8 mm (Fig. 4B). In the case of chaetognatha and krill distributions, both groups showed local maximum concentrations at St. 32 (10 600 and 909 ind. m^{-2}, respectively) (Fig. 3G). The size structure of krill shows a frequency peak around 5–7 mm ESD (Fig. 4B) (∼15 mm length) corresponding with larval/juvenile stages; in fact, the abundance of large individuals collected during the cruise could be underestimated due to net avoidance by adults (Wiebe *et al.*, 2013, and references therein).

Normalized biomass size spectra

The NBSS slopes of the plankton community (pico- to zooplankton) varied from −1.02 to −0.79, the steepest slope was found at the southern station (St. 11) (Fig. 3A). These slopes were significantly different from −1 (*t*-test, $t = 10.32$, $df = 21$, $P < 0.001$). Interestingly, a dome anomaly in the slopes of the size spectra was present at the size classes corresponding to 5–10 μm ESD which were dominated by small diatoms (Fig. 5). This anomaly was less pronounced north of the Shetland Front (Fig. 5B), and at both edges of the T.1b, where the MLDs reached maximum values (Table I) and the microplanktonic cells accumulate slightly <100 μm ESD (Fig. 5D and F). Moreover, within the zooplankton size range (>250 μm

Downloaded from http://plankt.oxfordjournals.org/ at Southern Methodist University on August 22, 2014

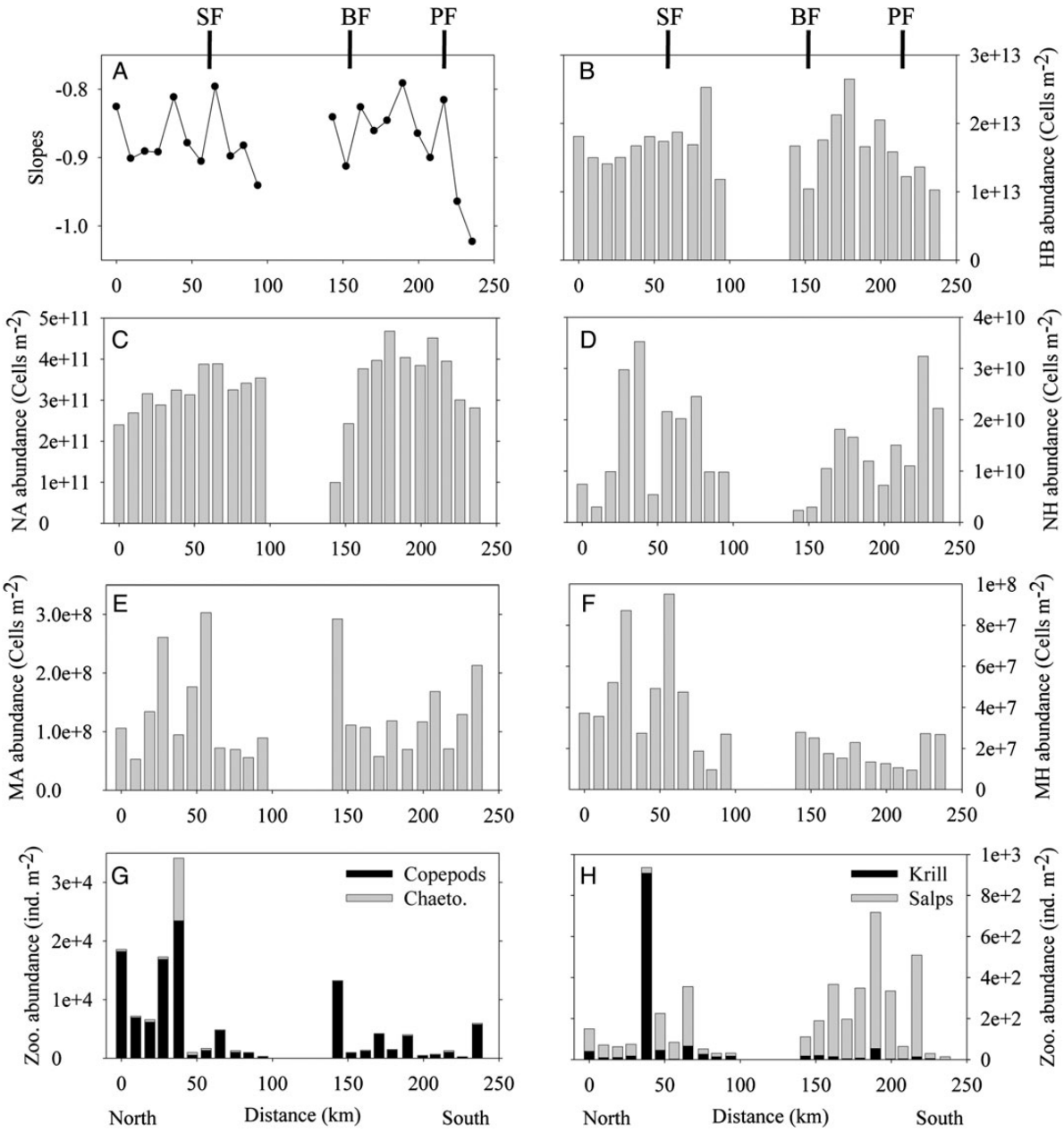

Fig. 3. NBSS slopes and the integrated abundances (cells m^{-2}) (**A**–**H**) of the different trophic compartments studied along the transect. HB: heterotrophic bacteria, NA: nanoautotrophs, NH: nanoheterotrophs, MA: microautotrophs, MH: microheterotrophs. The locations of the fronts are indicated above the upper panels: BF: Bransfield Front, PF: Peninsula Front, SF: Shetland Front.

ESD), a clear trough above the fitted NBSS was detected up to 2 mm ESD, whereas biomass seemed to accumulate towards the larger sizes (Fig. 5). Although domes and troughs were detected, R^2 showed a good linear fit with values always over 0.86 (F-test, $P < 0.001$); however, significant differences ($P < 0.05$) were detected in terms of intercept and slope between stations (Fig. 5), especially south of the Peninsula Front (Fig. 1). Pearson correlations performed between SST and the NBSS parameters showed significantly ($P < 0.05$) flatter spectra and lower intercept values as temperature increased ($r = 0.59$ and -0.46, respectively).

Metabolic rates

NPP rates showed a gradual increase southwards with a marked difference between T.1a (mean ± SD: 566 ± 268 mg C m^{-2} day^{-1}) and T.1b (1178 ± 492 mg C m^{-2} day^{-1}). An opposite trend was detected for CR rates

Downloaded from http://plankt.oxfordjournals.org/ at Southern Methodist University on August 22, 2014

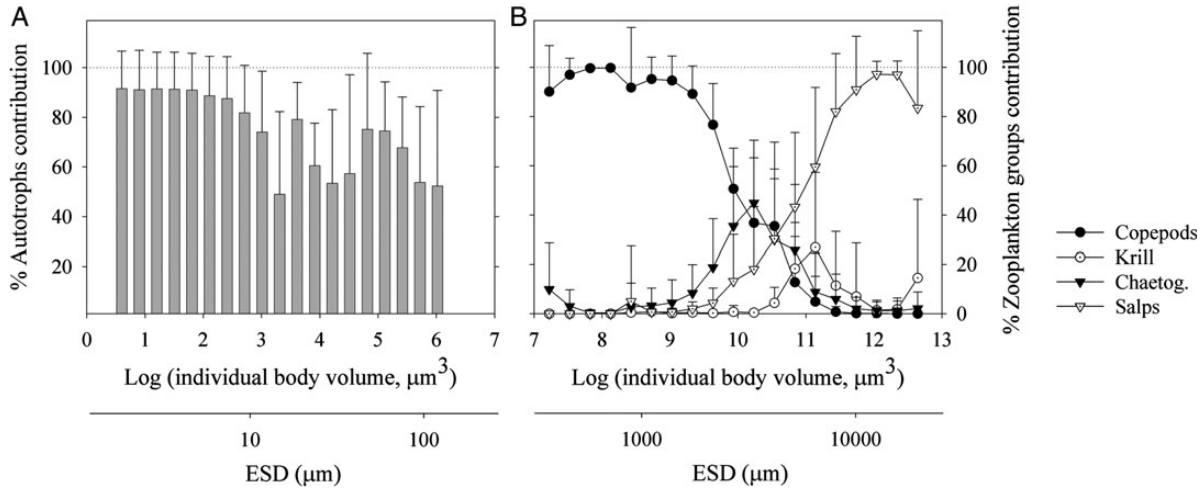

Fig. 4. (**A**) Average and standard deviation of autotrophic cells contribution (%) with respect to total biomass of each size class for all the stations sampled. (**B**) Average and standard deviation of the different zooplankton groups contribution (%) to total zooplankton biomass of each size class for all stations sampled.

(Table I), as north of the archipelago values reached 1233 ± 341 mg C m^{-2} day^{-1} and, in the Bransfield Strait, these respiration rates decreased to 696 ± 224 mg C m^{-2} day^{-1}. St. 5 represented an exception due to the high respiration rate detected (1068 mg C m^{-2} day^{-1}) (Table I) corresponding also with the highest NPP recorded (2193 mg C m^{-2} day^{-1}). GPP/CR ratio varied between 0.73 and 3.55, with values <1 (heterotrophic balance) on most of the northern leg and values mainly >2 in the Bransfield Strait showing that GPP exceeded CR along T.1b (Fig. 6A). Average values (surface down to 400 m) of $\%O_2$ have also been plotted on the same graph to examine trends across the transect (Fig. 6A). In the northern heterotrophic region, averaged $\%O_2$ remained low ($\approx 65-70\%$), whereas a clearly higher $\%O_2$ was detected in the autotrophic region.

Although phytoplankton respiration is, on average, 60.8% of total CR (Fig. 6B), significant ($P < 0.05$) negative correlations between heterotrophic respiration rates (from pico- to macro-size range) and the GPP/CR ratio revealed a strong control of the heterotrophic community on the total CR (Table II). In contrast, phytoplankton respiration rates significantly ($P < 0.05$) increased as the SST increased. Overall, although not significant ($P = 0.07$), a negative relationship ($r = -0.38$) was detected between SST and GPP/CR. NH respiration was, on average, 21.1% of total CR, followed by zooplankton (8.6%), HB (7.5%) and MH (1.0%) (Fig. 6B). To further discern a GPP threshold for our study area, we have performed a least-square linear regression between NCP and GPP data (Fig. 6C) (*F*-test, $F_{21} = 35.58$, $P < 0.001$) and resolved the curve fit for NCP = 0, obtaining a GPP threshold of 963 mg C m^{-2} day^{-1}. However, 35% of variability was explained by the relationship between NCP and CR; therefore, not only unproductive areas would result in a net heterotrophic state but also those stations where primary production and CR were uncoupled. If we transform GPP threshold into volumetric units, to compare with already published thresholds, assuming a PQ of 1.2 and a mean integration depth of 77 m (average integration depth calculated on the basis of MLD and Zeu, Table I), we obtained an estimated value of 1.25 mmol O_2 m^{-3} day^{-1}.

Spatial differentiation of the metabolic assemblages

The MDS ordination plot divided the stations into two similar groupings (Fig. 7) (clusters from 80% of similarity were isolated) with an optimal stress value (0.01). Cluster I was mainly composed of those stations situated north of the archipelago including St. 4 and 11 as well, where GPP/CR ratios nearly or below 1 were detected (heterotrophic community). In fact, within Cluster I, a transition between the northern stations, north of the Shetland Front and those situated close to the coast (St. 27 and 28) was detected. Therefore, Cluster II was mainly formed by those stations situated south of the archipelago, where GPP/CR ratios were >2 (autotrophic community). Within Cluster II, it was noteworthy that St. 2 and 9, where mesoscale fronts (Bransfield and Peninsula Front, respectively) were located (Fig. 1), were grouped together. Although all the trophic compartment abundances (log-transformed) were examined to discern patterns across the clusters identified, only significant relationships ($r > 0.5$, $P < 0.05$) with the MDS analysis were shown (Fig. 7).

Downloaded from http://plankt.oxfordjournals.org/ at Southern Methodist University on August 22, 2014

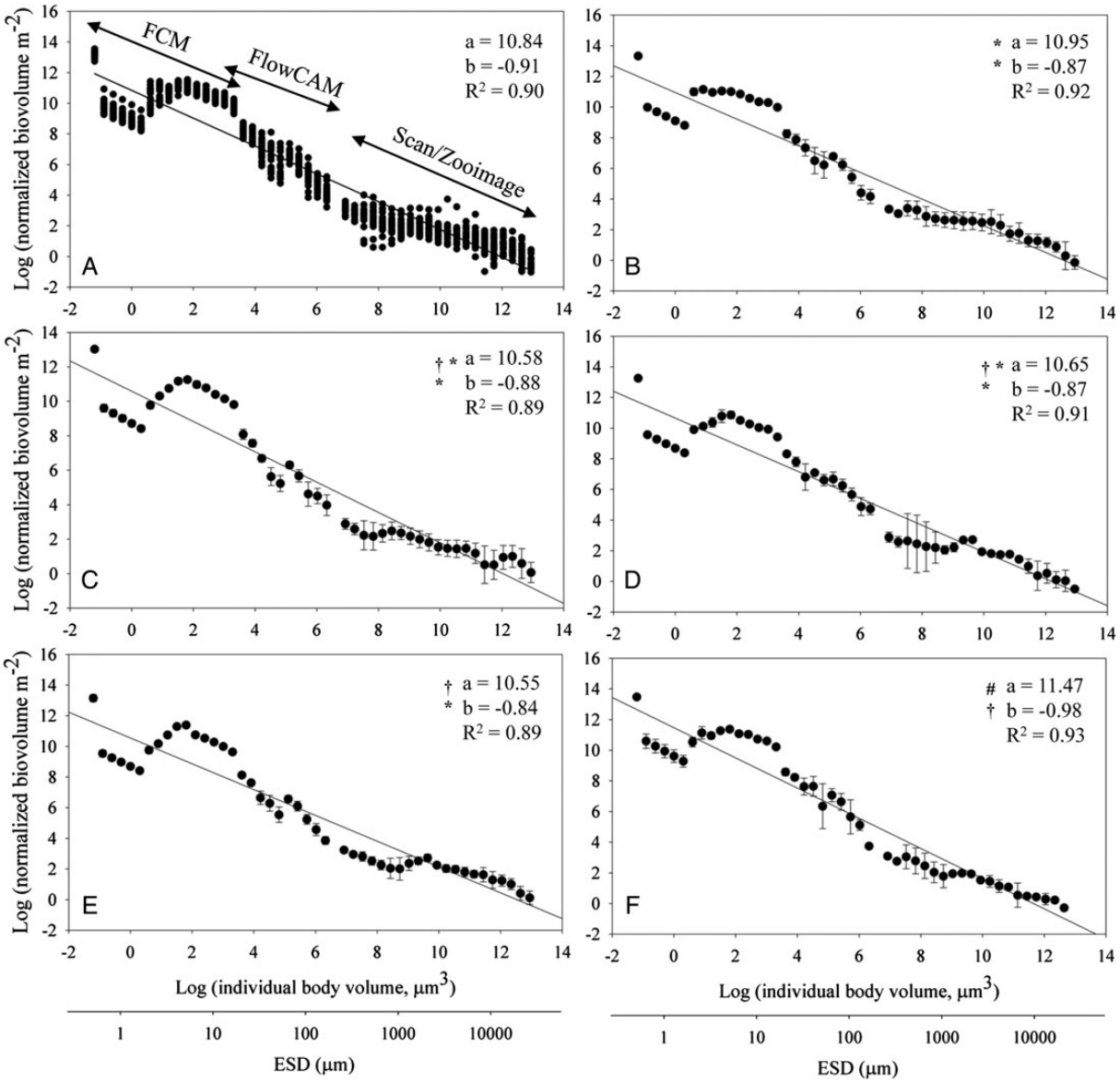

Fig. 5. Overall normalized biomass size macrospectrum for all stations sampled (**A**) and average (±SD) NBSS of dissimilar group of stations (**B**–**F**) according to the mesoscale structures location (Fig. 1). (B) North of the SF (St. 36–30); (C) Northern SSI shelf (St. 29–24); (D) From SSI to BF (St. 1–2); (E) Middle Bransfield Strait, from BF to PF (St. 3 to 9); (F) South of the PF (St. 10–11). Regions sharing symbols are not significantly different in terms of NBSS parameters (intercept and slope, respectively) (Tukey *post hoc* HSD tests, $P < 0.05$). A schematic of the techniques used to characterize each size range is represented on panel A. FCM: flow cytometry. Abbreviations as in Figs 1–3.

Higher MH, copepods and chaetognatha abundances characterized Cluster I while higher salp abundance characterized Cluster II. All the respiration rates significantly increased towards the northern stations (Cluster I).

DISCUSSION

In the context of an extreme and highly variable ecosystem, such as the Antarctic ecosystem, few studies (Witek and Krajewska-Soltys, 1989; Tarling *et al.*, 2012) have attempted to use the size spectra to obtain ecological information of the whole planktonic community. The large amount of data that should be measured and managed to build up a consistent spectrum is a major disadvantage of this method. However, as Platt and Denman (Platt and Denman, 1978) predicted, currently all regions of the biomass spectrum are accessible to rather automatic survey, so building up the planktonic NBSS is now easier than decades ago. The study of the planktonic size

Downloaded from http://plankt.oxfordjournals.org/ at Southern Methodist University on August 22, 2014

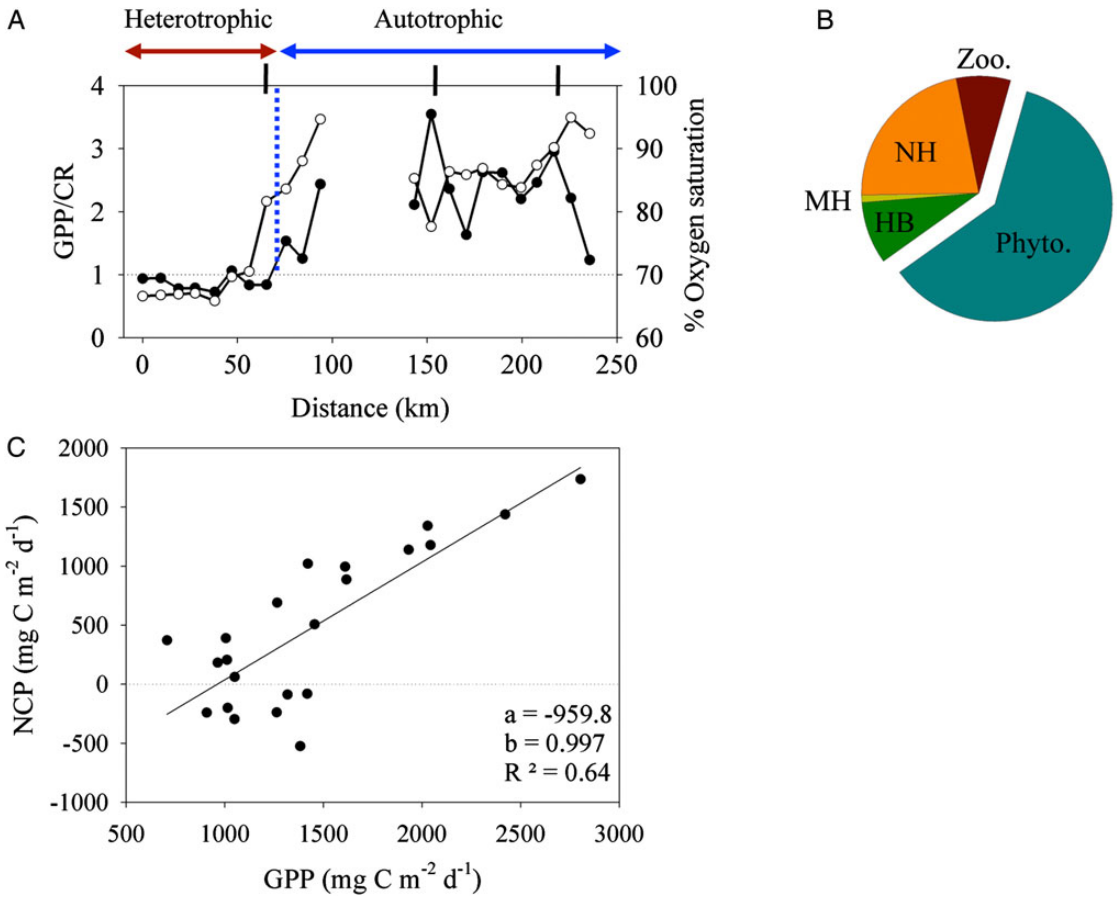

Fig. 6. (**A**) Gross primary production/community respiration (GPP/CR) ratio (black dots) and the average percentage of oxygen saturation ($\%O_2$) (surface down to 400 m) (white dots) modulation along the transect. The locations of the fronts are indicated above the figure. (**B**) The relative contribution to total respiration of the different trophic compartments. Percentages in the text above. (**C**) Relationship between net community production (NCP) and gross primary production (GPP) for the stations sampled. Standard errors: Slope = ± 255.7, Intercept = ± 0.17.

Table II: Pearson correlation coefficients among integrated respiration rates (log-transformed) and GPP/CR ratio and SST

$N = 22$	HB	Phytoplankton	NH	MH	Zooplankton
GPP/CR	**−0.63**	−0.42	**−0.75**	**−0.63**	**−0.45**
SST	−0.06	**0.61**	0.30	0.16	0.20

Numbers in bold are statistically significant, $P < 0.05$. Abbreviations as in Table I.

spectra is an valuable tool that allows us to overview in a synoptic way all the biological compartments involved (Kerr and Dickie, 2001) and observe their joint evolution either temporally or spatially (e.g. changes in carbon flux across the trophic levels, prey–predators interactions, community production–respiration ratios) and their responses to perturbation. In this study, we have emphasized spatial differences in the NBSS throughout a mesoscale north–south transect, as the Drake Passage–Bransfield Strait area is considered as a zone where a transition from an autotrophic to a heterotrophic budget takes place (e.g. Fig. 3a in Duarte *et al.*, 2013; Fig. 1 in Williams *et al.*, 2013).

On the other hand, in recent years, an intense effort has been made to address and investigate the discrepancy between metabolic balance data in different oceanic areas (e.g. Serret *et al.*, 2001a; Williams *et al.*, 2004; Mouriño-Carballido and McGillicuddy, 2006). The growing number of studies that encompass global data (Robinson and Williams, 2005; Duarte and Regaudie-de-Gioux, 2009; Duarte *et al.*, 2013) provide compelling evidence for the existence of a GPP threshold below which planktonic communities tend to be heterotrophic. In the case of the SO and specifically around the SSI, although the published data showed a net autotrophic community balance, low phytoplankton productivity areas linked to the predominance of a heterotrophic community have been described (Agustí *et al.*, 2004, and references therein). Using different approaches, Duarte and

Downloaded from http://plankt.oxfordjournals.org/ at Southern Methodist University on August 22, 2014

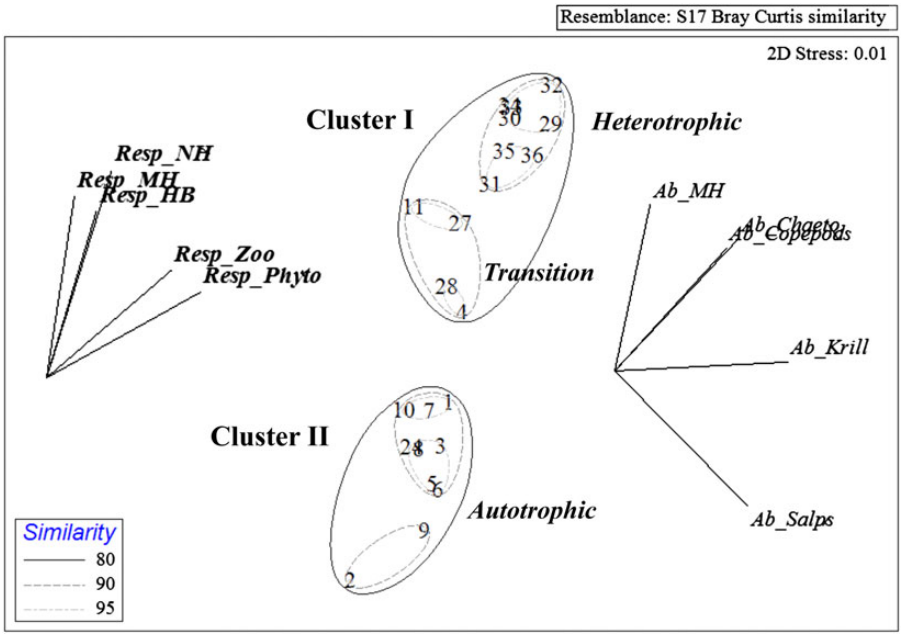

Fig. 7. MDS-cluster ordination analysis of the stations on the basis of NBSS slopes and metabolic balance. Significant Pearson rank correlation vectors of the strongest relationships ($r > 0.5$, $P < 0.05$) between integrated abundance (cells m^{-2}) (log-transformed) and respiration rates (mg C m^{-2} day^{-1}) (in bold) of the different trophic compartments and the MDS analysis were overlapped. HB: heterotrophic bacteria, NH: nanoheterotrophs, MH: microheterotrophs.

Regaudie-de-Gioux (Duarte and Regaudie-de-Gioux, 2009) reported a mean GPP threshold for the SO of 1.25 mmol O_2 m^{-3} day^{-1} equal to our estimated volumetric value and slightly lower than that reported by Agustí *et al.* (Agustí *et al.*, 2004). Therefore, we can establish this threshold as valid for our study area, which coupled to the size spectrum gives valuable information of the power of the plankton community to act either as a CO_2 source or sink. Although Duarte and Regaudie-de-Gioux (Duarte and Regaudie-de-Gioux, 2009) initially criticized the modelling approach used by López-Urrutia *et al.* (López-Urrutia *et al.*, 2006) to derive CR, we have highlighted the usefulness of these equations to obtain reliable respiration rates from smaller phytoplankton to larger zooplankton in the SO.

Methodological considerations

Some possible methodological limitations of the present study should be recognized in view of their potential influence on the NBSS. It is evident that one of the most complex issues when constructing size spectra that simultaneously cover a size range as wide as the one presented in this study is the operational difficulty of conducting perfect sampling and to use optimum preservation methods, as pointed out by Quiñones *et al.* (Quiñones *et al.*, 2003).

Gaps

Within the picoplankton size range, it is noteworthy that, in truly polar seas, picocyanobacteria are typically observed in negligible or low abundances. This fact has been ascribed to the cold-tolerant but not psychrophilic growth characteristics of high-latitude cyanobacteria and their inability to keep pace with loss processes such as advection and grazing in cold oceans (Scanlan, 2012, and references therein). Due to this lack of picoplanktonic phototrophic populations, no distinguishable groups could be observed in the flow cytometer scatterplots. It is possible that the measurements are approaching the detection limit of the instrument. In this sense, we filled up the biological gaps by applying the method proposed by Tittel *et al.* (Tittel *et al.*, 1998) but being even more restrictive within the picoplankton size range to ensure a realistic biomass distribution. However, a methodological gap between 200 and 250 μm due to the non-overlap of the techniques used was inevitable. Although the Platt and Denman model is sensitive to missing size ranges in the size spectrum, all depth-integrated complete community spectra showed a good linear fit with R^2 values always over 0.86. Several studies have determined losses for smaller taxa, especially copepods, using a 250-μm net (Gallienne and Robins, 2001, and references therein), however, during this cruise, we detected similar copepod abundances compared with the values reported during a previous cruise in the Bransfield Strait with different

Downloaded from http://plankt.oxfordjournals.org/ at Southern Methodist University on August 22, 2014

plankton nets (Hernández-León *et al.*, 2013). In this sense, Ward *et al.* (Ward *et al.*, 2012a) did not find a difference between nets (53, 100 and 200 μm) in terms of mesozooplankton biomass in Antarctic waters (see their Tables II and III). Furthermore, excluding the extreme size classes of both FlowCAM (158.8–200.1 μm ESD) and scanning (252.1–400.2 μm ESD) methods no significant differences (paired *t*-test, $P > 0.1$) were detected between the complete NBSS parameters (intercept and slope) in each area (Fig. 2) and the restricted NBSS; thus, we do not consider that smaller zooplankton was underrepresented and the upper and lower size classes of both methods, respectively, were finally included.

Functional groups and metabolic rates

Many dinoflagellates are photosynthetic but an equal number obtain their carbon by ingesting other phytoplankton and many are now being shown to be mixotrophic (Hacket *et al.*, 2004). Heterotrophic activity of some species classified as phytoplankton cannot be ruled out. Assuming all dinoflagellates to be autotrophs, we have probably overestimated the autotrophic metabolic rates in the microplankton fraction, which would lead us to conclude that the community balance could be slightly more heterotrophic than the results presented in this paper. Even if it were assumed that dinoflagellates were producing half of their potential production rate due to their size, if grazing upon other cells, the total production estimation slightly decreases by only 1.1%.

On the other hand, Regaudie-de-Gioux and Duarte (Regaudie-de-Gioux and Duarte, 2012) obtained an average E_a for CR, through a compilation of different datasets, much higher (1.03) than the one used in this study for heterotrophic respiration which can significantly decrease the respiration rates calculated here; however, other authors have reported E_a values similar to 0.56 for Antarctic waters (Martínez and Estrada, 1992; Arístegui and Montero, 1995a).

Integration depth

As shown in Thompson *et al.* (Thompson *et al.*, 2013), significant differences were detected in the zooplankton NBSS between day and night samples due to vertical migration. Several studies have focused on zooplankton diel migration in the Antarctic, especially copepods and krill (e.g. Hernández-León *et al.*, 2001; Nicol, 2006 and references therein); even salps have been described to undertake diel vertical migrations (Perissinotto and Pakhomov, 1998). In this sense, accurate spectra of the zooplankton size range should include a representative section of the water column, integration between surface and 400 m being a reasonable spatial compromise (Ward *et al.*, 2012a). In the case of cells smaller than 250 μm ESD, the integration depth was chosen in relation to physics. Swimming speeds of these small organisms are much lower than ambient fluid velocities and, consequently, behavioural movements have little effect on their larger scale distribution patterns (McManus and Woodson, 2012). The assumption that the mixed layer was actively mixing at the time of sampling has been shown by Sangrà *et al.* (Sangrà *et al.*, 2014). However, we must also take into account that the euphotic zone often extends below the mixed layer (Table I) where respiration tends to be high relative to GPP (Regaudie-de-Gioux and Duarte, 2010). As a consequence, we considered to depth integrate the NBSS and, therefore, the metabolic rates within the euphotic zone or the MLD, whichever was deeper, throughout the transect. We should also consider that several authors have reported abundant microzooplankton <100 m in Antarctic Waters (e.g. Alder and Boltovskoy, 1993); however, a recent comprehensive study performed by Garzio *et al.* (Garzio and Steinberg, 2013) throughout the Western Antarctic Peninsula revealed rapid decrease of microzooplankton abundance below the depth of the *in situ* fluorescence maximum, which in this study was always above the MLD or the Zeu (García-Muñoz *et al.*, 2013a, 2014).

Plankton community structure

NBSS data presented in this paper provide a summer snapshot. Although presumably representative of the planktonic community of the region, it should be not taken as that of the community in steady-state conditions both due to temporal–seasonal and fortuitous variations linked to hydrodynamic spatial structures at a shorter scale. In fluctuating, uncoupled, aquatic systems, characterized by irregularities in the NBSS, the steady-state spectrum could be obtained by making a seasonal integration of states (García *et al.*, 1995), but, in this case, equivalent data for the winter season were not available. In the same way, the hydrography and circulation of the Drake Passage–Bransfield Strait region is complex and variable (e.g. García *et al.*, 2002; Zhou *et al.*, 2002; Sangrà *et al.*, 2011). Therefore, the uncoupling between trophic compartments and the strong influence of hydrodynamic processes (e.g. Varela *et al.*, 2002; Hewes *et al.*, 2009; Hernández-León *et al.*, 2013) could reflect spatial changes in the NBSS and, moreover, a metabolic uncoupling between production and respiration rates. The community structure found along the north–south transect crossing the SSI was consistent with the results presented in Witek and Krajewska-Soltys (Witek and Krajewska-Soltys, 1989). Far from being a steady-state system, it may be seen as disturbed due to its uneven planktonic NBSS. This dome-like pattern due to the

Downloaded from http://plankt.oxfordjournals.org/ at Southern Methodist University on August 22, 2014

predominance of nanoplanktonic phytoplankton cells and the scarcity of picoplankton during the summer season was widely observed by Rodríguez *et al.* (Rodríguez *et al.*, 2002) and Zabala (Zabala, 2005) in the Bransfield and Gerlache Strait. Moreover, flat slopes throughout the selected transect revealed high biomass transfer efficiency through higher trophic levels. As described by Tarling *et al.* (Tarling *et al.*, 2012), even when other seasons were considered, the shallowness of the Antarctic NBSS slope may be an effect of longevity and life cycles on trophic interactions in Antarctic waters.

Metabolic state: physical/biological interactions

In this study a clear spatial segregation between stations north (Cluster I) and south (Cluster II) of the archipelago was detected in terms of the NBSS shape and the GPP/CR ratio (Fig. 7). The metabolic state north of the SSI seemed to be almost net heterotrophic while south of the archipelago an autotrophic state prevailed. This spatial pattern is attributable to several factors. On one hand, a southwards increase of NPP, driven by a nutrient limitation in the northern stations (García-Muñoz *et al.*, 2013b) and the presence of physical features (fronts and eddies) that modulate the MLD and hence the accumulation of phytoplankton (García-Muñoz *et al.*, 2013a). It is well known that one of the mechanisms that could generate pulses of net autotrophy is associated with mesoscale eddies (Mouriño-Carballido and McGillicuddy, 2006). In fact, the highest GPP/CR ratios were detected related with these physical features (Table I, Fig. 7).

On the other hand, the heterotrophic budget detected north of the archipelago, especially north of the Shetland Front, is attributable to a northwards increase of CR due to: (i) a higher phytoplankton respiration activity as temperature increases and (ii) a higher presence of heterotrophic organisms (microheterotrophs, chaetognaths and copepods) along T.1a (Fig. 7). Overall, all the trophic compartments increased their respiration rates northwards (Fig. 7); thus, a sum of physical and biological processes appears to act synergistically. In this sense, the $\%O_2$ has been used as an indicator of this contrasting pattern, the SF being an apparent boundary between net heterotrophic and autotrophic communities (Figs 2 and 6). The $\%O_2$ vertical distribution revealed relatively higher oxygen consumption in deeper layers of the Drake area where the highest copepod abundances were detected. However, upper layers elsewhere always showed high saturation percentages (even $>100\%$) connected with the higher presence of autotrophic cells (García-Muñoz *et al.*, 2013a). The oxygen super-saturation is interpreted as the consequence of net autotrophy producing excess oxygen, most of which is lost by gas exchange to the atmosphere (Ducklow and Doney, 2013).

The role of water temperature in the distribution and production of planktonic organisms has been widely studied in the SO. However, few studies have been made to relate their respiration rates to temperature probably due to methodological considerations as argued in Williams *et al.* (Williams *et al.*, 2013). A plausible solution could be linked to the use of indirect methods of respiration measurement, as we propose in this paper via the joint application of NBSS and MTE equations. MTE predicts that respiration rates should rise more rapidly than GPP as temperature increases (Allen *et al.*, 2005; Harris *et al.*, 2006; López-Urrutia *et al.*, 2006). This corollary fits with the results presented in Regaudie-de-Gioux and Duarte (Regaudie-de-Gioux and Duarte, 2012) using dark-light *in vitro* metadata. This results, in turn, in a decline in the GPP/CR ratio for planktonic communities with increasing temperature as we have detected due to the significant increase of phytoplankton respiratory activity. North of the SSI, no CR data have ever been measured, so we cannot compare with the results presented in this paper, but CR rates measured in the Bransfield Strait were in the range of those previously reported (e.g. $0.45-1.69$ g C m^{-2} day^{-1} in Arístegui and Montero, 1995b). Several authors have related CR with chlorophyll a (Martínez and Estrada, 1992; Arístegui and Montero, 1995b; Regaudie-de-Gioux and Duarte, 2013) suggesting that phytoplankton make a major contribution to total CR. In this study, first, we have found that phytoplankton cells dominated the total biomass of micro-organisms (Fig. 4) and second, we have quantified that their respiration rates represents on average, 60.8% of total CR increasing significantly as SST increase. These results both confirm the hypothesis of Karl *et al.* (Karl *et al.*, 1991) and the results presented in Lefèvre *et al.* (Lefèvre *et al.*, 2008) that phytoplankton are responsible for much of the heterotrophic microbial metabolism in coastal Antarctic waters during summer and the fact that low variations in temperature could significantly affect plankton respiratory activity (Vosjan and Olanczuk-Neyman, 1991).

Furthermore, the role of consumers (microbes and zooplankton) in the metabolic balance and carbon export flux should be considered. The calculated bacterial respiration rates agree with the reduced rates described during periods of high phytoplankton production (Wiebe *et al.*, 1992). Although only six bacterial respiration rates were measured during our cruise (see Teira *et al.*, 2012), these *in situ* measurements agreed with the low calculated rates obtained by using the López-Urrutia and Morán (López-Urrutia and Morán, 2007) equation (Equation 3). Several prior studies have reported that bacterial respiration is a relatively small fraction of CR in

Downloaded from http://plankt.oxfordjournals.org/ at Southern Methodist University on August 22, 2014

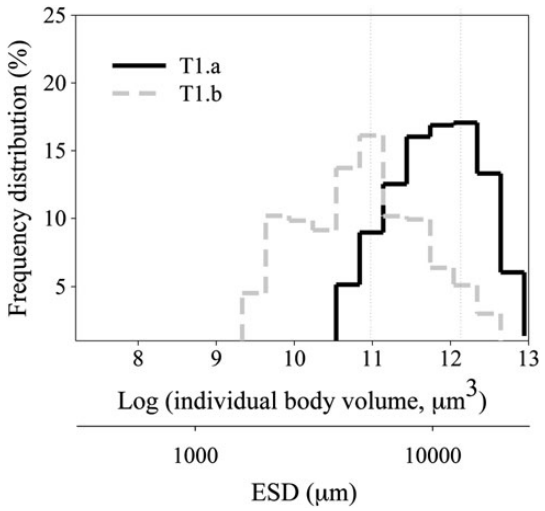

Fig. 8. Average salp size frequency distribution (%) on both sides of the SSI.

Antarctic waters (e.g. Arístegui *et al.*, 1996) and Ducklow *et al.* (Ducklow *et al.*, 2000) stated that it should be ≈10% CR, as we have observed. Thus, bacterial metabolism seems to have a secondary role in the global planktonic metabolic balance in the study area.

Conversely, mesozooplankton abundance strongly correlated with the identified metabolic clusters (Fig. 7), salps being the group that characterized the southern stations grouping where they contributed up to 40% of total mesozooplankton abundance. Mesozooplankton activity appears to strongly influence the vertical transport in the study area as reflected by the high number of faecal pellets encountered in the Bransfield Strait (Serret *et al.*, 2001b; Anadón *et al.*, 2002). Salps by producing large, fast sinking faecal pellets may be major contributors to the downward particulate carbon flux (Fortier *et al.*, 1994; Le Fèvre *et al.*, 1998; Perissinotto and Pakhomov, 1998). Especially, the smaller salp specimens (<30 mm) may possibly be on average 2.4-fold more efficient in re-packaging suspended particles than larger (>30 mm) salps (Pakhomov, 2004). Using the individual size frequency distribution, a clear-size shift towards smaller individuals was detected south of the archipelago (T.1b) (Fig. 8), as previously reported (Huntley *et al.*, 1989). Therefore, south of the SSI, energy would not be successfully transferred from primary production to higher trophic levels, but would sink and be buried into the deep ocean, as previously described by Arístegui and Montero (Arístegui and Montero, 1995b) and Anadón *et al.* (Anadón *et al.*, 2002).

In light of the results, the planktonic community structure, and not only the photosynthetic organisms, influences the degree of autotrophy/heterotrophy of the Antarctic planktonic ecosystem. At this point, we must emphasize that both GPP/CR ratios and biological abundances shown in this study represented a summer snapshot and therefore are not representative of long-term averages. In this sense, Agustí *et al.* (Agustí *et al.*, 2004) argue this to be a product of a bias toward the study of bloom conditions.

Overall, the variations in the biovolume spectra and metabolic rates in a given region are influenced by short-term physical and biological processes such as advection and grazing (Zhou *et al.*, 2004) or successional or seasonal stages of the community. The behaviour of the system is linked to ice dynamics not only on a seasonal scale, but also experiencing inter-annual variations in the duration and extent of sea ice cover. In fact, the region studied is experiencing rapid climate warming (Stammerjohn *et al.*, 2008) that can modify its dynamics by modifying the abundance, production, distribution and composition of the different trophic levels. In order to evaluate better the metabolic budget and its variations, and to have an improved integrative view of this changing system, it would be useful to analyse changes in size structure across different states. It would be good to compare states from other seasons and years as well as validate respiration estimations obtained with allometric models based on on-board experiments. This would lead to a more complete view of metabolic budgets in this region around the Antarctic Peninsula.

ACKNOWLEDGEMENTS

We are grateful to the captain, crew and scientists on board the R.V. Hespérides for their co-operation and logistic support during the cruise. Thanks are also given to Eduardo Ramírez for his assistance in analysing plankton samples and to Beatriz Mouriño and María Pérez for the oxygen sensor calibration. We greatly thank María Lidia Nieves for her dedication and patience analysing zooplankton samples.

FUNDING

This work was supported by project COUPLING CTM2008-06343-C02-02/ANT from the Spanish Ministry of Science and Education. C.G-M.'s work was supported by a pre-doctoral fellowship from the Spanish Council for Research (CSIC), JAE-Predoc 2009.

REFERENCES

Agustí, S. and Duarte, C. M. (2005) Threshold of gross primary production for planktonic metabolic balance in the Southern Ocean: an experimental test. *Limnol. Oceanogr.*, **50**, 1334–1339.

Downloaded from http://plankt.oxfordjournals.org/ at Southern Methodist University on August 22, 2014

Agustí, S., Satta, M. P. and Mura, M. P. (2004) Summer community respiration and pelagic metabolism in upper surface Antarctic waters. *Aquat. Microb. Ecol.*, **35**, 197–205.

Alcaraz, M., Saiz, E., Calbet, A. *et al.* (2003) Estimating zooplankton biomass through image analysis. *Mar. Biol.*, **143**, 307–315.

Alder, V. A. and Boltovskoy, D. (1993) The ecology of microzooplankton in the Weddell-Scotia Confluence area: horizontal and vertical distribution patterns. *J. Mar. Res.*, **51**, 323–344.

Allen, A. P., Gillooly, J. F. and Brown, J. H. (2005) Linking the global carbon cycle to individual metabolism. *Ecology*, **19**, 202–213.

Álvarez, E., López-Urrutia, A., Nogueira, E. *et al.* (2011) How to effectively sample the plankton size spectrum? A case study using FlowCAM. *J. Plankton Res.*, **33**, 1119–1133.

Anadón, R., Alvarez-Marqués, F., Fernández, E. *et al.* (2002) Vertical biogenic flux during Austral summer in the Antarctic Peninsula area. *Deep-Sea Res. II*, **49**, 883–901.

Anadón, R. and Estrada, M. (2002) The FRUELA cruises. A carbon flux study in productive areas of the Antarctic Peninsula (December 1995-February 1996). *Deep-Sea Res. II*, **49**, 567–583.

Arístegui, J. and Montero, M. F. (1995a) The relationship between community respiration and ETS activity in the ocean. *J. Plankton Res.*, **17**, 1563–1571.

Arístegui, J. and Montero, M. F. (1995b) Plankton community respiration in Bransfield Strait (Antarctic Ocean) during austral spring. *J. Plankton Res.*, **17**, 1647–1659.

Arístegui, J., Montero, M. F., Ballesteros, S. *et al.* (1996) Planktonic primary production and microbial respiration measured by ^{14}C assimilation and dissolved oxygen changes in coastal waters of the Antarctic Peninsula during austral summer: implications for carbon flux studies. *Mar. Ecol. Prog. Ser.*, **132**, 191–201.

Atkinson, A., Meyer, B., Stübing, D. *et al.* (2002) Feeding and energy budgets of Antarctic krill *Euphausia superba* at the onset of winter: II. Juveniles and adults. *Limnol. Oceanogr.*, **47**, 953–966.

Bachiller, E. and Fernandes, J. A. (2011) Zooplankton image analysis manual: automated identification by means of scanner and digital camera as imaging devices. *Rev. Invest. Mar.*, **18**, 16–37.

Behrenfeld, M. J., Boss, E., Siegel, D. A. *et al.* (2005) Carbon-based ocean productivity and phytoplankton physiology from space. *Global Biogeochem. Cycles*, **19**, GB1006. doi:10.1029/2004GB002299.

Black, A. R. and Dodson, S. I. (2003) Ethanol: a better preservation technique for *Daphnia*. *Limnol. Oceanogr. Methods.*, **1**, 45–50.

Blanco, J. M., Quiñones, R. A., Guerrero, F. *et al.* (1998) The use of biomass spectra and allometric relations to estimate respiration of planktonic communities. *J. Plankton Res.*, **20**, 887–900.

Calbet, A., Alcaraz, M., Atienza, D. *et al.* (2005) Zooplankton biomass distribution patterns along the western Antarctic Peninsula (December 2002). *J. Plankton Res.*, **27**, 1195–1203.

Carrillo, C. J., Smith, R. C. and Karl, D. M. (2004) Processes regulating oxygen and carbon dioxide in surface waters west of the Antarctic Peninsula. *Mar. Chem.*, **84**, 161–179.

Christaki, U., Courties, C., Massana, R. *et al.* (2011) Optimized routine flow cytometric enumeration of heterotrophic flagellates using SYBR Green I. *Limnol. Oceanogr. Methods.*, **9**, 329–339.

Church, M. J., De Long, E. F., Ducklow, H. W. *et al.* (2003) Abundance and distribution of planktonic *Archaea* and *Bacteria* in the waters west of the Antarctic Peninsula. *Limnol. Oceanogr.*, **48**, 1893–1902.

Cózar, A., García, C. M. and Gálvez, J. A. (2003) Analysis of plankton size spectra irregularities in two subtropical shallow lakes (Esteros del Iberá, Argentina). *Can. J. Fish. Aquat. Sci.*, **60**, 411–420.

Culberson, C. H. (1994) Dissolved oxygen. In WOCE Operations Manual. Vol. 3: The Observational Program. Section 3.1: WOCE Hydrographic Program. Part 3.1.3; WHP Operations and Methods. WHP Office Report WHPO 91–1/WOCE Report No. 68/91. Woods Hole, MA.

del Giorgio, P. A., Bird, D. F., Prairie, Y. T. *et al.* (1996) Flow cytometric determination of bacterial abundance in lake plankton with the green nucleic acid stain SYTO 13. *Limnol. Oceanogr.*, **41**, 783–789.

Delille, D. (2003) Seasonal and inter-annual variability of bacterioplankton biomass at station Kerfix, off Kerguelen Islands, Antarctica. *Oceanol. Acta*, **26**, 225–229.

Duarte, C. M. and Regaudie-de-Gioux, A. (2009) Thresholds of gross primary production for the metabolic balance of marine planktonic communities. *Limnol. Oceanogr.*, **54**, 1015–1022.

Duarte, C. M., Regaudie-de-Gioux, A., Arrieta, J. M. *et al.* (2013) The oligotrophic ocean is heterotrophic. *Ann. Rev. Mar. Sci.*, **5**, 551–569.

Ducklow, H. W., Dickson, M.-L., Kirchman, D. L. *et al.* (2000) Constraining bacterial production, conversion efficiency and respiration in the Ross Sea, Antarctica, January-February, 1997. *Deep-Sea Res. II*, **47**, 3227–3247.

Ducklow, H. W. and Doney, S. C. (2013) What is the metabolic state of the oligotrophic ocean? A debate. *Annu. Rev. Mar. Sci.*, **5**, 525–533.

Fortier, L., Le Fèvre, J. and Legendre, L. (1994) Export of biogenic carbon to fish and to the deep ocean: the role of large planktonic microphages. *J. Plankton Res.*, **16**, 809–839.

Gaedke, U. (1993) Ecosystem analysis based on biomass size distributions: a case study of plankton community in a large lake. *Limnol. Oceanogr.*, **38**, 112–127.

Gallienne, C. P. and Robins, D. B. (2001) Is *Oithona* the most important copepod in the world's ocean? *J. Plankton Res.*, **23**, 1421–1432.

García, C. M., Echevarría, F. and Niell, F. X. (1995) Size structure of plankton in a temporary, saline inland lake. *J. Plankton Res.*, **17**, 1803–1817.

García, M. A., Castro, C. G., Ríos, A. F. *et al.* (2002) Water masses and distribution of physico-chemical properties in the Western Bransfield Strait and Gerlache Strait during Austral summer 1995/96. *Deep-Sea Res. II*, **49**, 585–602.

García-Muñoz, C. (2014) Physical-biological coupling around the South Shetland Islands (Antarctica): dynamics, distribution and size structure of the planktonic community. Ph.D. thesis, Univ. of Cádiz.

García-Muñoz, C., López-Urrutia, A., Lubián, L. M. *et al.* (2013b) A comparison of primary production models in an area of high mesoscale variability (South Shetland Islands, Antarctica). *J. Sea Res.*, **83**, 30–39.

García-Muñoz, C., Lubián, L. M., García, C. M. *et al.* (2013a) A mesoscale study of phytoplankton assemblages around the South Shetland Islands (Antarctica). *Polar Biol.*, **36**, 1107–1123.

García-Muñoz, C., Sobrino, C., Lubián, L. M. *et al.* (2014) Factors controlling phytoplankton physiological state around the South Shetland Islands (Antarctica). *Mar. Ecol. Prog. Ser.*, **498**, 55–71.

Garzio, L. M. and Steinberg, D. K. (2013) Microzooplankton community composition along the Western Antarctic Peninsula. *Deep-Sea Res. I*, **77**, 36–49.

Hacket, J. D., Anderson, D. M., Erdner, D. L. *et al.* (2004) Dinoflagellates: a remarkable evolutionary experiment. *Am. J. Bot.*, **91**, 1523–1534.

Harris, L. A., Duarte, C. M. and Nixon, S. W. (2006) Allometric laws and prediction in estuarine and coastal ecology. *Estuaries Coasts*, **29**, 340–344.

Downloaded from http://plankt.oxfordjournals.org/ at Southern Methodist University on August 22, 2014

Hernández-León, S. and Ikeda, T. (2005) A global assessment of mesozooplankton respiration in the ocean. *J. Plankton Res.*, **27**, 153–158.

Hernández-León, S., Portillo-Hahnefeld, A., Almeida, C. *et al.* (2001) Diel feeding behaviour of krill in the Gerlache Strait, Antarctica. *Mar. Ecol. Prog. Ser.*, **223**, 235–242.

Hernández-León, S., Sangrà, P., Lehette, P. *et al.* (2013) Zooplankton biomass and metabolism in the frontal zones of the Bransfield Strait, Antarctica. *J. Marine Syst.*, **111–112**, 196–207.

Hewes, C. D., Reiss, C. S. and Holm-Hansen, O. (2009) A quantitative analysis of sources for summertime phytoplankton variability over 18 years in the South Shetland Islands (Antarctica). *Deep-Sea Res. I*, **56**, 1230–1241.

Huntley, M. E., Sykes, P. F. and Marin, V. (1989) Biometry and trophodynamics of *Salpa thompsoni* foxton (Tunicata: Thaliacea) near the Antarctic Peninsula in austral summer, 1983–1984. *Polar Biol.*, **10**, 59–70.

Kara, A. B., Rochford, P. A. and Hurlburt, H. E. (2000) An optimal definition for ocean mixed layer depth. *J. Geophys. Res.*, **105**, 16803–16821.

Karl, D. M., Holm-Hansen, O., Taylor, G. T. *et al.* (1991) Microbial biomass and productivity in the western Bransfield Strait, Antarctica during the 1986–87 austral summer. *Deep-Sea Res. II*, **38**, 1029–1055.

Kerr, S. R. and Dickie, L. M. (2001) *The Biomass Spectrum. A Predator-Prey Theory of Aquatic Production*. Columbia University Press, New York.

Kremer, P. and Madin, L. P. (1992) Particle retention efficiency of salps. *J. Plankton Res.*, **1**, 1009–1015.

Laws, E. A. and Archie, J. W. (1981) Appropriate use of regression analysis in marine biology. *Mar. Biol.*, **65**, 13–16.

Lefèvre, D., Guigue, C. and Obernesterer, I. (2008) The metabolic balance at two contrasting sites in the Southern Ocean: the iron fertilized Kerguelen area and HNLC waters. *Deep-Sea Res. II*, **55**, 766–776.

Le Fèvre, J., Legendre, L. and Rivkin, R. B. (1998) Fluxes of biogenic carbon in the Southern Ocean: roles of large microphagous zooplankton. *J. Marine Syst.*, **17**, 325–345.

Loeb, V., Hofmann, E. E., Klinck, J. M. *et al.* (2010) Hydrographic control of the marine ecosystem in the South Shetland-Elephant Island and Bransfield Strait region. *Deep-Sea Res. II*, **57**, 519–542.

López-Urrutia, A. and Morán, X. A. (2007) Resource limitation of bacterial production distorts the temperature dependence of oceanic carbon cycling. *Ecology*, **88**, 817–822.

López-Urrutia, A., San Martín, E., Harris, R. P. *et al.* (2006) Scaling the metabolic balance of the oceans. *PNAS*, **103**, 8739–8744.

Martínez, R. and Estrada, M. (1992) Respiratory electron transport activity of microplankton in the Weddell Sea during early spring: influence of the ice cover and the ice edge. *Polar Biol.*, **12**, 275–282.

McManus, M. A. and Woodson, C. B. (2012) Plankton distribution and ocean dispersal. *J. Exp. Biol.*, **215**, 1008–1016.

Menden-Deuer, S. and Lessard, E. J. (2000) Carbon to volume relationships for dinoflagellates, diatoms, and other protist plankton. *Limnol. Oceanogr.*, **45**, 569–579.

Menden-Deuer, S., Lessard, E. J. and Satterberg, J. (2001) Effect of preservation on dinoflagellate and diatom cell volume and consequences for carbon biomass predictions. *Mar. Ecol. Prog. Ser.*, **222**, 41–50.

Meyer, B., Atkinson, A., Stubing, D. *et al.* (2002) Feeding and energy budgets of Antarctic krill *Euphausia superba* at the onset of winter: I. Furcilia III larvae. *Limnol. Oceanogr.*, **47**, 943–952.

Mouriño-Carballido, B. and McGillicuddy, D. J. (2006) Mesoscale variability in the metabolic balance of the Sargasso Sea. *Limnol. Oceanogr.*, **51**, 2675–2689.

Nicol, S. (2006) Krill, currents, and sea ice: *Euphausia superba* and its changing environment. *Bioscience*, **56**, 111–120.

Pakhomov, E. A. (2004) Salp/krill interactions in the eastern Atlantic sector of the Southern Ocean. *Deep-Sea Res. II*, **51**, 2645–2660.

Perissinotto, R. and Pakhomov, E. A. (1998) Contribution of salps to carbon flux of marginal ice zone of the Lazarev Sea, Southern Ocean. *Mar. Biol.*, **131**, 25–32.

Platt, T. and Denman, K. (1978) The structure of pelagic ecosystems. *Rapp. P.-V. Reun. Cons. Perm. Int. Explor. Mer.*, **173**, 60–65.

Quiñones, R. A., Blanco, J. M., Echevarría, F. *et al.* (1994) Metabolic size-spectra from an oceanographic station off Fuengirola, Spain. *Sci. Mar.*, **58**, 53–58.

Quiñones, R. A., Platt, T. and Rodríguez, J. (2003) Patterns of biomass-size spectra from oligotrophic waters of the Northwest Atlantic. *Prog. Oceanogr.*, **57**, 405–427.

Regaudie-de-Gioux, A. and Duarte, C. M. (2010) Compensation irradiance for planktonic community metabolism in the ocean. *Global Biogeochem. Cycles*, **24**, GB4013. doi:10.1029/2009GB003639.

Regaudie-de-Gioux, A. and Duarte, C. M. (2012) Temperature dependence of planktonic metabolism in the ocean. *Global Biogeochem. Cycles*, **26**, GB1015. doi:10.1029/2010GB003907.

Regaudie-de-Gioux, A. and Duarte, C. M. (2013) Global patterns in oceanic planktonic metabolism. *Limnol. Oceanogr.*, **58**, 977–986.

Reul, A., Rodríguez, J., Blanco, J. M. *et al.* (2006) Control of microplankton size structure in contrasting water columns of the Celtic Sea. *J. Plankton Res.*, **28**, 449–457.

Robinson, C. and Williams, P. J. le B. (2005) Respiration and its measurement in surface marine waters. In del Giorgio, P. A. and Williams, P. J. le B. (eds), *Respiration in Aquatic Ecosystems*. Oxford Univ. Press, New York, pp. 147–181.

Rodhouse, P. G., Piatkowski, U., Murphy, E. J. *et al.* (1994) Utility and limits of biomass spectra—the nekton community sampled with the RMT25 in the Scotia Sea during austral summer. *Mar. Ecol. Prog. Ser.*, **112**, 29–39.

Rodríguez, J., Jiménez-Gómez, F., Blanco, J. M. *et al.* (2002) Physical gradients and spatial variability of the size structure and composition of phytoplankton in the Gerlache Strait (Antarctica). *Deep-Sea Res. II*, **49**, 693–706.

Rodríguez, J. and Mullin, M. (1986) Relation between biomass and body weight of plankton in a steady state oceanic ecosystem. *Limnol. Oceanogr.*, **31**, 361–370.

Sangrà, P., García-Muñoz, C., García, C. M. *et al.* (2014) Coupling between the upper ocean layer variability and size-fractionated phytoplankton in a no nutrient environment. *Mar. Ecol. Prog. Ser.*, **499**, 35–46.

Sangrà, P., Gordo, C., Hernádez-Arencibia, M. *et al.* (2011) The Bransfield current system. *Deep-Sea Res. I*, **58**, 390–402.

San Martín, E. (2005) Latitudinal variation in plankton size spectra along the Atlantic Ocean. PhD Thesis. Univ. of Southampton.

Scanlan, D. J. (2012) Marine picocyanobacteria. In Whitton, B. A. (ed.), *Ecology of Cyanobacteria II, Their Diversity in Space and Time*. Springer, London, pp. 503–534.

Serret, P., Fernández, E., Anadón, R. *et al.* (2001b) Trophic control of biogenic carbon export in Bransfield and Gerlache Straits, Antarctica. *J. Plankton Res.*, **23**, 1345–1360.

Downloaded from http://plankt.oxfordjournals.org/ at Southern Methodist University on August 22, 2014

Serret, P., Robinson, C., Fernández, E. *et al.* (2001a) Latitudinal variation of the balance between plankton photosynthesis and respiration in the eastern Atlantic Ocean. *Limnol. Oceanogr.*, **46**, 1642–1652.

Sheldon, R. W., Prakash, A. and Sutcliffe, W. H. Jr (1972) The size distribution of particles in the ocean. *Limnol. Oceanogr.*, **17**, 327–340.

Shin, Y.-J., Rocher, M.-J., Jennings, S. *et al.* (2005) Using size-based indicators to evaluate the ecosystem effects of fishing. *ICES J. Mar. Sci.*, **62**, 384–396.

Sokal, R. R. and Rohlf, F. J. (1981) *Biometry: the Principles and Practice of Statistics in Biological Research*, 2nd edn. W. H. Freeman and Company, San Francisco.

Sprules, W. G. and Munawar, M. (1986) Plankton size spectra in relation to ecosystem productivity, size, and perturbation. *Can. J. Fish. Aquat. Sci.*, **43**, 1789–1794.

Stammerjohn, S. E., Martinson, D. G., Smith, R. C. *et al.* (2008) Sea ice in the Western Antarctic Peninsula region: spatio-temporal variability from ecological and climate change perspectives. *Deep Sea Res. II*, **55**, 2041–2058.

Tarling, G. A., Stowasser, G., Ward, P. *et al.* (2012) Seasonal trophic structure of the Scotia Sea pelagic ecosystem considered through biomass spectra and stable isotope analysis. *Deep-Sea Res. II*, **59–60**, 222–236.

Teira, E., Mouriño-Carballido, B., Martínez-García, S. *et al.* (2012) Primary production and bacterial carbon metabolism around South Shetland Islands in the Southern Ocean. *Deep-Sea Res. I*, **69**, 70–81.

Thompson, G. A., Dinofrio, E. O. and Alder, V. A. (2013) Structure, abundance and biomass size spectra of copepods and other zooplankton communitites in upper waters of the Southwestern Atlantic Ocean during summer. *J. Plankton Res.* doi:10.1093/plankt/fbt014.

Tittel, J., Zippel, B., Geller, W. *et al.* (1998) Relationships between plankton community structure and plankton size distribution in lakes of northern Germany. *Limnol. Oceanogr.*, **43**, 1119–1132.

Varela, M., Fernández, E. and Serret, P. (2002) Size-fractionated phytoplankton biomass and primary production in the Gerlache and south Bransfield straits (Antarctic Peninsula) in Austral summer 1995–1996. *Deep-Sea Res. II*, **49**, 749–768.

Vosjan, J. H. and Olanczuk-Neyman, K. M. (1991) Influence of temperature on respiratory ETS-activity of micro-organisms from Admiralty Bay, King George Island. Antarctica. Nerh. *J. Sea Res.*, **28**, 221–225.

Ward, P., Atkinson, A. and Tarling, G. (2012a) Mesozooplankton community structure and variability in the Scotia Sea: a seasonal comparison. *Deep-Sea Res. II*, **59–60**, 78–92.

Ward, P., Atkinson, A., Venables, H. *et al.* (2012b) Food web structure and bioregions in the Scotia Sea: a seasonal synthesis. *Deep-Sea Res. II*, **59–60**, 253–266.

Weiss, R. F. (1970) The solubility of nitrogen, oxygen and argon in water and seawater. *Deep-Sea Res.*, **17**, 721–735.

Westberry, T., Behrenfeld, M. J., Siegel, D. A. *et al.* (2008) Carbon-based primary productivity modeling with vertically resolved photoacclimation. *Global Biogeochem. Cycles*, **22**, GB2024. doi:10.1029/2007GB003078.

Wiebe, P. H., Lawson, G. L., Lavery, A. C. *et al.* (2013) Improved agreement of net and acoustical methods for surveying euphausiids by mitigating avoidance using a net-based LED strobe light system. *ICES J. Mar. Sci.* doi:10.1093/icesjms/fst005.

Wiebe, W. J., Sheldon, J. R. and Pomeroy, L. R. (1992) Bacterial growth in the cold: evidence for an enhanced substrate requirement. *Appl. Environ. Microbiol.*, **58**, 359–364.

Williams, P. J. le B., Morris, P. J. and Karl, M. (2004) Net community production and metabolic balance at the oligotrophic ocean site, station ALOHA. *Deep-Sea Res. I*, **51**, 1563–1578.

Williams, P. J. le B., Quay, P. D., Westberry, T. K. *et al.* (2013) The oligotrophic ocean is autotrophic. *Annu. Rev. Mar. Sci.*, **5**, 535–549.

Witek, Z. and Krajewska-Soltys, A. (1989) Some examples of epipelagic plankton size structure in high latitude oceans. *J. Plankton Res.*, **11**, 1143–1155.

Zabala, L. (2005) Estudio del picoplankton y nanoplankton fototrópico en el ecosistema antártico. PhD Thesis, Univ. of Málaga.

Zhou, M., Niiler, P. P. and Hu, J. -H. (2002) Surface currents in the Bransfield and Gerlache Straits, Antarctica. *Deep-Sea Res. I*, **49**, 267–280.

Zhou, M., Zhu, Y. and Peterson, J. D. (2004) *In situ* growth and mortality of mesozooplankton during the austral fall and winter in Marguerite Bay and its vicinity. *Deep-Sea Res. II*, **51**, 2099–2118.

Zubkov, M. V., Burkill, P. H. and Topping, J. N. (2007) Flow cytometric enumeration of DNA-stained oceanic planktonic protists. *J. Plankton Res.*, **29**, 79–86.

Downloaded from http://plankt.oxfordjournals.org/ at Southern Methodist University on August 22, 2014